Mon. Not. R. Astron. Soc. **367,** 323–330 (2006) doi:10.1111/j.1365-2966.2005.09952.x

5-GHz MERLIN and VLBA observations of compact 9C sources

R. C. Bolton,[1⋆] C. J. Chandler,[2] G. Cotter,[3] T. J. Pearson,[4] G. G. Pooley[1⋆]
A. C. S. Readhead,[4] J. M. Riley[1⋆] and E. M. Waldram[1⋆]

[1]*Cavendish Astrophysics, Department of Physics, Madingley Road, Cambridge CB3 0HE*
[2]*National Radio Astronomy Observatory, PO Box 0, Socorro, NM 87801, USA*
[3]*Oxford Astrophysics, Denys Wilkinson Building, Keble Road, Oxford OX1 3RH*
[4]*California Institute of Technology, 1200 East California Blvd, Pasadena, CA 91125, USA*

Accepted 2005 December 2. Received 2005 November 23; in original form 2005 September 29

ABSTRACT

In this paper, we present subarcsecond resolution observations of 36 compact sources from the 15^h region of the 15-GHz 9th Cambridge survey. These sources all have previously measured simultaneous continuum radio spectra spanning 1.4–43 GHz and we classify each source by fitting a quadratic function to its spectrum. Using the Multi-Element Radio-Linked Interferometer Network and the Very Long Baseline Array, both at 5 GHz, we resolve all six steep-spectrum objects and four of the 13 flat-spectrum objects. However, none of the 16 objects with convex spectra peaking above 2.5 GHz is resolved even at <3-mas resolution. These results, in combination with the findings of a 15-GHz variability study, suggest that emission from the high-frequency peaking objects is affected by relativistic beaming, and that these objects are not necessarily as young as the synchrotron self-absorption interpretation of their peak frequencies would imply.

Key words: surveys – galaxies: active – radio continuum: general.

1 INTRODUCTION

This is the second paper in a series discussing the results of follow-up observations of sources taken from the 15-GHz 9th Cambridge survey (9C: Waldram et al. 2003). The main scientific motivation for 9C was the need to identify contaminant foreground sources in the fields of the cosmic microwave background experiment using the Very Small Array (Taylor et al. 2003). 9C should be representative of the whole sky at 15 GHz and so provides a unique view of the radio source population at high frequency and low flux density levels (9C is complete to ∼25 mJy or lower in some regions). Extensive radio and optical observations of 176 sources from 9C have been carried out using the Very Large Array (VLA) and the Ryle Telescope (RT) at radio wavelengths and the 60-inch optical telescope at the Palomar Observatory. This work is presented by Bolton et al. (2004) (Paper 1 hereafter), and it provides simultaneous continuum radio spectra spanning 1.4–43 GHz for all the objects, and an optical identification for ∼90 per cent of them. 19 per cent of the sources in a sample complete to 25 mJy in 9C had spectra with fitted peak frequencies between 0.5 and 10 GHz which is double the fraction found in lower frequency (e.g. 5 GHz) surveys (O'Dea 1998).

Synchrotron self-absorption models (e.g. O'Dea 1998) predict that very young (younger than a few thousand years) compact radio sources should be optically thick and have spectra rising up to gigahertz or a few gigahertz frequencies. Thus sources peaking at higher frequency are more dense, smaller and younger than sources peaking at lower frequency, so high-frequency peaked-spectrum (HFP) objects may represent the youngest population of radio sources.

Two thirds of the 9C sources studied in Paper 1 were unresolved by the VLA. Higher-resolution observations are, therefore, required in order to map the structure of these sources, especially the flat- and peaked-spectrum objects which are more often compact than the steep-spectrum objects. These should help to establish whether the peaked-spectrum objects in this sample resemble classical double radio sources in their infancy or if they are instead beamed objects.

In this paper, we present subarcsecond resolution data for 36 of the sources in the RA ∼15^h follow-up field that are unresolved by the VLA data in Paper 1. The VLA maps of sources in the 15^h field in Paper 1 have synthesized beams at 43 GHz of approximately 2 arcsec. These maps include visibilities from a few long baselines so structure smaller than 2 arcsec in some sources has been resolved but poorly mapped.

Two sets of high-resolution observations were made, first with the Multi-Element Radio-Linked Interferometer Network (MERLIN) in 2002 November–December and then, for sources still unresolved with MERLIN, with the Very Long Baseline Array (VLBA) in 2004 February. All observations were made at 5 GHz, at which frequency the MERLIN array has a resolution of 50 mas and the VLBA a resolution of ∼2.5 mas.

Our aim was to select all sources less than 2 arcsec in extent in the VLA maps for further study. However, source selection was

⋆E-mail: r.c.bolton.97@cantab.net (RCB); guy@mrao.cam.ac.uk (GGP); julia@mrao.cam.ac.uk (JMR); emw1@mrao.cam.ac.uk (EMW)

Table 1. Radio sizes and flux densities from the VLA, MERLIN and VLBA data. The spectral classification from the simultaneous VLA data is also given. See text for explanation of columns 9 and 10.

Source	Spectral	Size (arcsec)			5-GHz flux density (mJy)			Notes	
(J2000)	class	VLA	MERLIN	VLBA	VLA	MERLIN	VLBA	Variability	Resolved
J1459+4442	HFP	<2.0	<0.05	<0.003	230 ± 10	240 ± 16	214 ± 13	V(P3)	
J1501+4537	HFP	<2.0	<0.05	<0.003	11.0 ± 0.5	11.7 ± 0.7	8.1 ± 0.6	V(P3)	
J1502+3753	Steep	3	3.0	–	127 ± 5	59.0 ± 10.4	–	N(P3)	R
J1502+3956	Flat	<2.0	<0.05	0.016	68.0 ± 1.2	46.9 ± 2.4	33.7 ± 3.0	–	R
J1503+4528	Steep	0.5	0.7	–	159 ± 5	178 ± 9.1	–	–	R
J1506+4359	HFP	<2.0	<0.05	<0.003	74.6 ± 1.5	74.2 ± 3.7	59 ± 6.7	V?	H?
J1506+3730	Flat	<2.0	–	0.016	770 ± 15	–	474 ± 26	V(P3)	R
J1506+4239	HFP	<2.0	<0.05	<0.003	552.8 ± 11	634 ± 35	536 ± 33	V(NED)	
J1510+4138	HFP	<2.0	<0.05	<0.003	41.9 ± 1.0	53.0 ± 3.3	40 ± 3.6	V?	
J1516+4349	Flat	<2.0	<0.05	<0.003	25.1 ± 0.3	23.0 ± 2.3	20.0 ± 1.8	V?	H?
J1516+3650	Flat	<2.0	<0.05	<0.003	105.0 ± 5.0	63.1 ± 3.2	60 ± 3.6	N(P3)	H?
J1517+3936	Flat	<2.0	<0.05	<0.003	26.0 ± 1.0	17.0 ± 0.9	16 ± 1.3	V(P3)	H?
J1518+4131	Flat	<2.0	<0.05	<0.003	27.1 ± 0.6	14.2 ± 0.8	10.2 ± 0.9	V(NED)	H?
J1519+4254	Flat	<2.0	<0.05	<0.003	67.2 ± 1.3	60.8 ± 3.1	67.3 ± 3.7	V(NED)	
J1519+3913	Steep	<2.0	0.16	–	103 ± 3	96 ± 5.2	–	N(P3)	R
J1520+3843	Steep	<2.0	<0.05	0.015	112.0 ± 2.2	50.7 ± 3.2	45.6 ± 3.0	N(P3)	R
J1520+4211	Flat	<2.0	<0.05	<0.003	56.5 ± 1.1	74.2 ± 4.2	34.9 ± 2.4	V(P3)	
J1521+4336	HFP	<2.0	<0.05	<0.003	423.7 ± 8.5	389 ± 19	260 ± 14	V(NED)	H?
J1526+3712	HFP	<2.0	<0.05	<0.003	72.0 ± 2.0	60.6 ± 3.1	49.5 ± 3.2	N(P3);V(NED)	H?
J1526+4201	HFP	<2.0	<0.05	<0.003	59.9 ± 1.2	71.5 ± 3.6	55.5 ± 3.2	V?	
J1528+3738	Steep	0.7	1.1	–	336 ± 20	250 ± 51	–	N(P3)	R
J1528+3816	HFP	<2.0	<0.05	<0.003	46.0 ± 1.0	30.2 ± 1.9	72 ± 11	V(P3)	
J1528+4233	Steep	<2.0	<0.05	0.005	57.2 ± 1.2	64 ± 4.4	61.2 ± 4.0	–	R
J1530+3758	GPS	<2.0	<0.05	<0.003	135.0 ± 3.0	127.3 ± 6.4	112.8 ± 5.7	N(P3)	H?
J1531+4356	GPS	<2.0	<0.05	<0.003	55.0 ± 1.0	68.7 ± 3.4	56.5 ± 3.3	V(NED)	
J1538+4225	Flat	<2.0	<0.05	0.008	40.5 ± 0.8	39.1 ± 2.0	34.6 ± 2.6	–	R
J1540+4138	HFP	<2.0	<0.05	<0.003	30.9 ± 0.6	40.3 ± 2.1	27.8 ± 2.9	V?	
J1545+4130	Flat	<2.0	0.53	–	56.8 ± 1.1	30 ± 3.4	–	–	R
J1547+4208	GPS	<2.0	<0.05	<0.003	71.0 ± 1.4	73.8 ± 3.7	80 ± 6.4	V(NED)	
J1548+4031	Flat	<2.0	<0.05	<0.003	60.0 ± 1.2	64.6 ± 3.3	62.4 ± 3.3	Constant	
J1550+4536	GPS	<2.0	<0.05	<0.003	60.0 ± 1.2	75.5 ± 3.8	67.3 ± 4.0	V(NED)	
J1550+4545	Flat	<2.0	<0.05	<0.003	17.9 ± 1.2	14.9 ± 0.9	11 ± 1.1	V?	H?
J1553+4039	GPS	<2.0	<0.05	<0.003	43.0 ± 1.0	40.2 ± 2.0	45.5 ± 2.5	Constant	
J1554+4350	HFP	<2.0	<0.05	<0.003	33.2 ± 0.6	32.5 ± 1.9	34 ± 2.6	Constant	
J1554+4348	GPS	<2.0	<0.05	<0.003	60.8 ± 1.2	62.3 ± 3.2	44.7 ± 3.6	V?	H?
J1557+4007	Flat	<2.0	<0.05	<0.003	87.0 ± 5.0	86.5 ± 4.4	84 ± 8.1	Constant	

made when the VLA data analysis was incomplete. There are seven sources less than 2 arcsec in extent that were initially thought to be extended due to the presence of what we subsequently assumed to be unassociated near neighbours. These seven were omitted from the high-resolution follow-up. One of these seven is resolved in the VLA data (and has an angular size of 1 arcsec) but the others only have upper limits on their size of 2 arcsec.

A study of the variability at 15 GHz of a subsample of the 9C follow-up sources from Paper 1 has been conducted over the past 3 yr and the results will be presented by Bolton et al. (submitted) (Paper 3 hereafter). In the discussion that follows, we make use of the information about the variability of some of these sources.

2 MERLIN OBSERVATIONS

MERLIN observations were carried out at intervals between 2002 November 16 and December 23. The absolute flux scale was calibrated using either 2134+004 or OQ208. Because this scaling is stable over periods of a few days routine observations of the gain calibrators are made each day or so; for any given observing run, or set of runs, the most appropriate gain calibrator observations are used (e.g. those closest in time and observed in good conditions). By comparing the flux densities of calibrator sources over different time ranges and by checking against the MERLIN calibrator flux density data base, the relative flux calibration is estimated to be accurate to about 2 per cent, though the absolute flux calibration is likely to be good only to 5–10 per cent.

A number of different phase calibration sources were used, with one close to the current target source observed every 5 min.

The MERLIN array has baselines in the range 85–3650 kλ at 5.0 GHz. It is, therefore, sensitive to surface brightness variations on angular scales from ∼1 arcsec down to ∼50 mas. Structure larger than ∼1 arcsec will be resolved out by the array.

After initial gain calibration and fringe fitting the MERLIN data were self-calibrated and mapped using the National Radio Astronomy Observatories (NRAO) AIPS package. Self-calibration of the phase or both amplitude and phase was carried out for individual sources detected with a sufficiently high signal-to-noise ratio. All maps were made with the AIPS task IMAGR using data from all baselines and with robust = 0 (intermediate between natural and uniform weighting), resulting in a beam of $\sim 50 \times 48$ mas^2, unless otherwise stated.

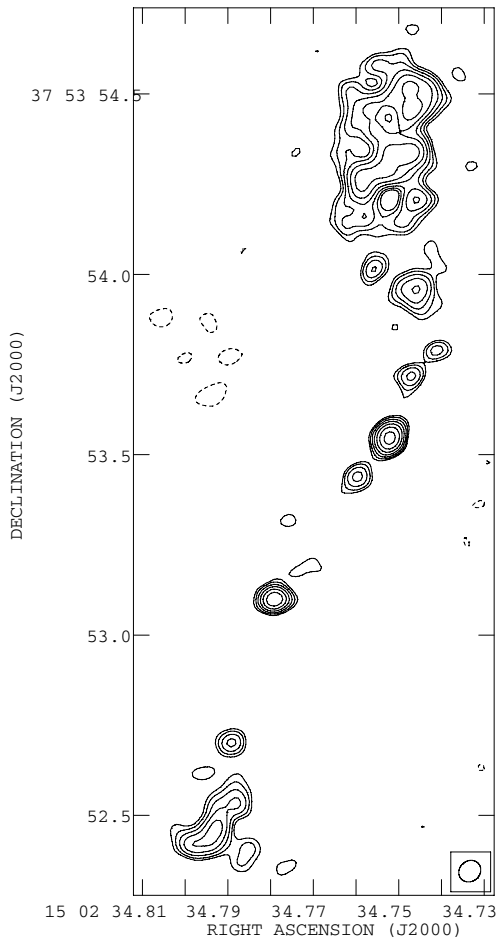

Figure 1. J1502+3753 mapped with MERLIN, using robust = 5. Contours $0.24 \times (-1, 1, \sqrt{2}, 2, 2\sqrt{2}, 4, ...)$ mJy beam^{-1}. Peak flux density 2.3 mJy beam^{-1}.

2.1 MERLIN results

The observed angular sizes and flux densities of the MERLIN sources are shown in Table 1. The flux density uncertainties include contributions from a 5 per cent assumed flux calibration uncertainty and the statistical uncertainty in measuring the flux density in each map.

Contour plots for the five sources that appear to be extended in their MERLIN maps are shown in Figs 1–5. In all cases the lowest positive contour is three times the rms off-source noise.

The extended sources are generally lower in flux density in the MERLIN maps than in the VLA maps which is expected when structure is resolved out. The exception is J1503+4528 which increases in flux density by 12 per cent. This source was resolved in the VLA map (see Paper 1), but the long-baseline *uv* coverage was poor so this increase is possibly due to differing *uv* coverage of the two maps rather than any intrinsic change.

J1502+3753 (Fig. 1) is a steep-spectrum source. There was some evidence of a weak second component ∼2 arcsec to the west of the main component in the VLA map at 4.8 GHz. The VLA map also showed some evidence for more extended emission in the north–south direction, but at very low levels of significance so the object was studied with MERLIN. The MERLIN map confirms the extended emission in the north–south direction but does not reveal a component to the west of the main jet.

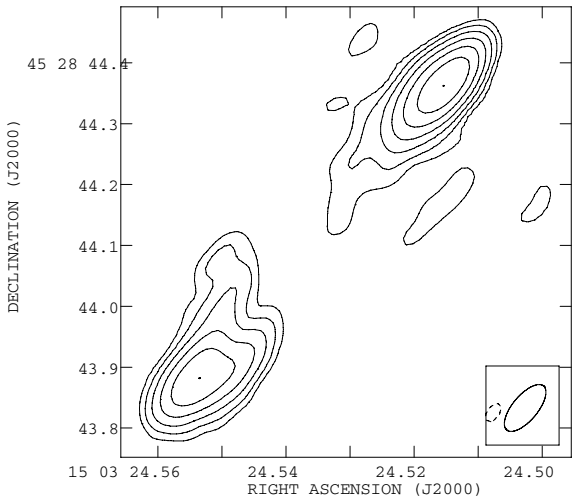

Figure 2. J1503+4528 mapped with MERLIN. Contours $0.96 \times (-1, 1, 2, 4, 8, ...)$ mJy beam^{-1}. Peak flux density 61.8 mJy beam^{-1}.

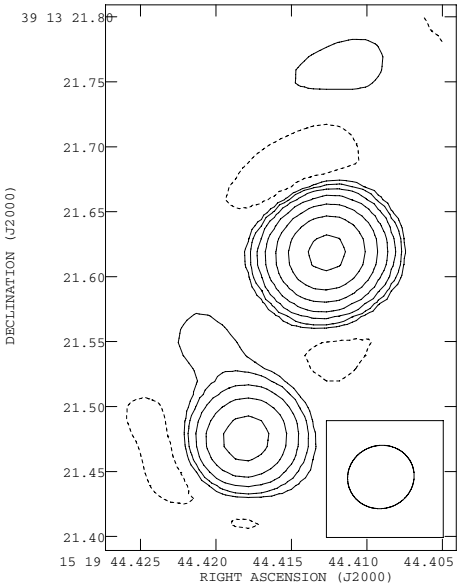

Figure 3. J1519+3913 mapped with MERLIN. Contours $0.93 \times (-1, 1, 2, 4, 8, ...)$ mJy beam^{-1}. Peak flux density 74.8 mJy beam^{-1}.

J1503+4528 (Fig. 2) was just resolved in the VLA 4.8-GHz data. The MERLIN data show that this is an asymmetric double source with two slightly resolved lobes, 0.7-arcsec apart with flux densities of 104 ± 3 and 74 ± 2 mJy.

J1519+3913 (Fig. 3) was not resolved in the VLA maps but the MERLIN image shows two unresolved components separated by 0.16 arcsec. Their flux densities are 74.8 ± 1.6 and 21.4 ± 0.7 mJy. This map is slightly noisy and we assume that the weak component to the north of the bright component is spurious.

J1528+3738 (Fig. 4) was slightly resolved with the VLA, and the MERLIN image reveals a core-jet structure about 1 arcsec in extent.

J1545+4130 (Fig. 5) was not resolved by the VLA. The MERLIN image shows a linear feature about 0.5 arcsec in angular extent; unusually for a flat-spectrum source it has no obvious compact core. It is not clear what the linear feature represents; it could be a compact

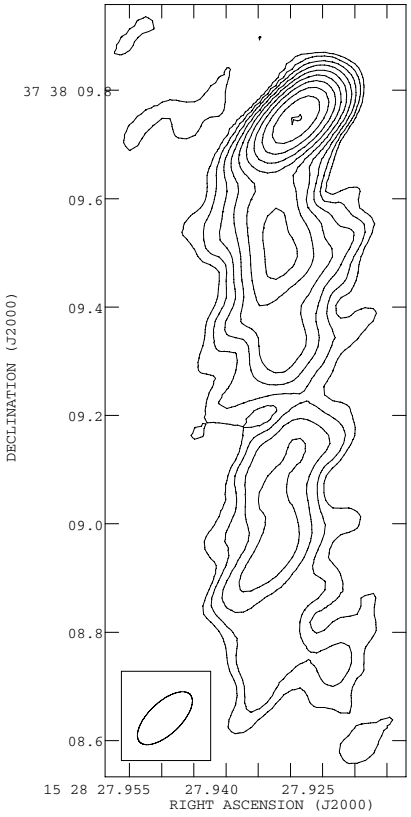

Figure 4. J1528+3738 mapped with MERLIN. Contours $3.9 \times (-1, 1, \sqrt{2}, 2, 2\sqrt{2}, 4, ...)$ mJy beam^{-1}. Peak flux density 89.9 mJy beam^{-1}.

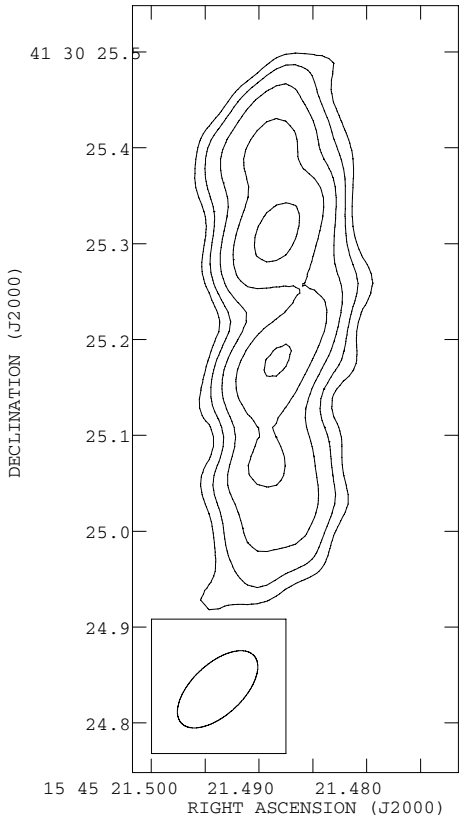

Figure 5. J1545+4130 mapped with MERLIN, using robust = 5. Contours $0.9 \times (-1, 1, \sqrt{2}, 2, 2\sqrt{2}, 4, ...)$ mJy beam^{-1}. Peak flux density 4.1 mJy beam^{-1}.

double source or a one- or two-sided jet with no associated core. The VLA flux density of J1545+4130 was significantly higher than that measured with MERLIN, suggesting that the source may have some faint emission on scales larger than ∼1 arcsec.

3 VLBA OBSERVATIONS

The VLBA observations were made in 2004 February 6, during one 12-h run. Bright 'fringe-finder' calibrators were observed at the beginning and throughout the run to allow calibration of the delays between antennas. Several different phase calibrators were used to enable fast slewing between the source and calibrator. Phase calibrators were observed for about 50 s after every 2 min on source. At 5 GHz the VLBA has baselines in the range $(2–143) \times 10^6\lambda$, so it is sensitive to surface brightness variations on scales from 90 down to 1.3 mas. All the VLBA data were reduced using the NRAO AIPS package. Maps were cleaned using the AIPS task IMAGR. By default maps were made with ROBUST = 0, but to obtain better sensitivity to extended structure some maps were made with a restricted *uv*-range and with ROBUST = 5 (natural weighting). The default mapping procedure resulted in a beam of $\sim 2.5 \times 1.5$ mas^2.

3.1 VLBA results

The flux densities and angular sizes measured with the VLBA are given in Table 1, with the VLA and MERLIN measurements. The VLBA flux density uncertainties include contributions from a 5 per cent flux calibration uncertainty and the statistical uncertainty in measuring the flux density in each map.

Five further sources were resolved by the VLBA: their contour plots are shown in Figs 6–10 where the lowest positive contour is at three times the rms noise off-source.

J1502+3956 (Fig. 6) is a 16-mas double radio source. No emission is detected connecting the two components. The north-east component has flux density 18.0 ± 1.2 mJy, and is not significantly resolved. The south-west component is resolved and has a total flux density of 15.7 ± 2.5 mJy. The flux density decreases from the VLA (68 mJy) to the MERLIN (46.9 mJy) and then to the VLBA (33.7 mJy) observations, which suggests that the source could have some diffuse extended structure that is being resolved out with increasing resolution.

J1506+3730 (Fig. 7) is a 16-mas core-jet source used as a phase calibrator for the VLBA observations. Its emission is dominated by the core (hence its suitability for use as a phase calibrator), with the extended emission at the level of a few per cent of the peak. There is a significant reduction in flux density in the VLBA map relative to the VLA map. It was found to be variable at 15 GHz at a level of 8 per cent over ∼3 yr in the study presented in Paper 3. Fomalont et al. (2000) observed J1506+3730 in their study of a large number of bright VLBA calibrators and their map shows that it is ≈12 mas in extent, with a much better signal-to-noise ratio than for the map shown here. Fomalont et al. (2000) measure a total flux density of ∼1 Jy. Both their map (data taken in 1996) and that of Taylor et al. (1996) (data taken in 1992) do not show the north-east (upper left-hand side) extension close to the core, so this source is clearly active.

J1520+3843 (Fig. 8) is 15 mas in extent, showing a possible jet structure.

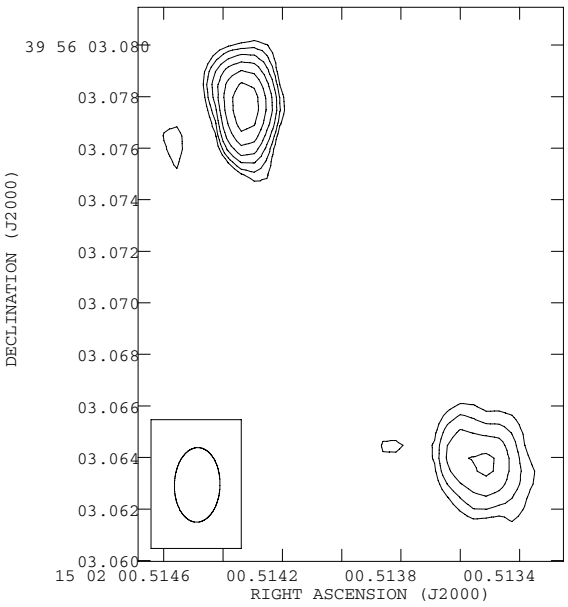

Figure 6. J1502+3956 mapped with the VLBA. Contours $2.4 \times (-1, 1, \sqrt{2}, 2, 2\sqrt{2}, 4, ...)$ mJy beam^{-1}. Peak flux density 17.4 mJy beam^{-1}.

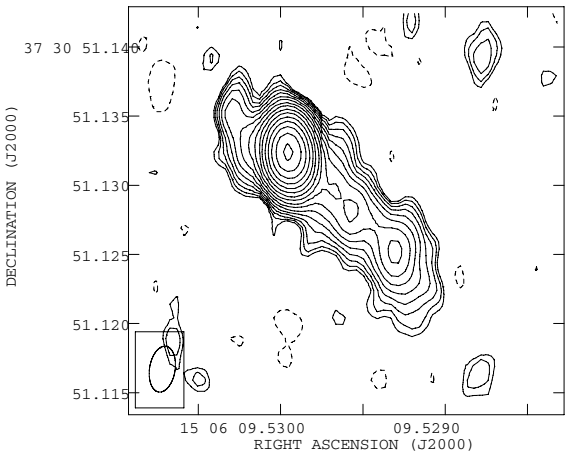

Figure 7. J1506+3730 mapped with the VLBA, using robust = 5. Contours $1.4 \times (-1, 1, \sqrt{2}, 2, 2\sqrt{2}, 4, ...)$ mJy beam^{-1}. Peak flux density 278.6 mJy beam^{-1}.

J1528+4233 (Fig. 9) is an extended, steep-spectrum source 5 mas in extent, just resolved by the VLBA.

The map of J1538+4225 (Fig. 10) shows possible weak extended structure to the west of the brightest component. The map is noisy and it is possible that the apparent structure results from phase errors (this source is too faint to allow self-calibration).

4 DISCUSSION

4.1 Radio spectral classification

Table 1 summarizes the high-resolution radio data, and the spectral class of each source. To classify sources according to their simultaneous radio spectra, a quadratic function [of the form $\log(S/\mathrm{mJy}) = A[\log(\nu/\mathrm{GHz})]^2 + B\log(\nu/\mathrm{GHz}) + C$] was fitted to the flux density data points from each of the 176 sources in Paper 1. The value of A is a measure of the curvature of the fitted spectrum (larger negative values of A corresponding to more convex spectral shapes). For a convex spectrum the fitted peak frequency is given by $\log(\nu/\mathrm{GHz}) = -B/(2A)$ and the spectral index α (where $S \propto \nu^{-\alpha}$) at 10 GHz is given by $\alpha_{10} = -(B + 2A)$. We define four spectral classes on the basis of the peak frequency, the spectral index at 10 GHz and the value of A found from this quadratic fit.

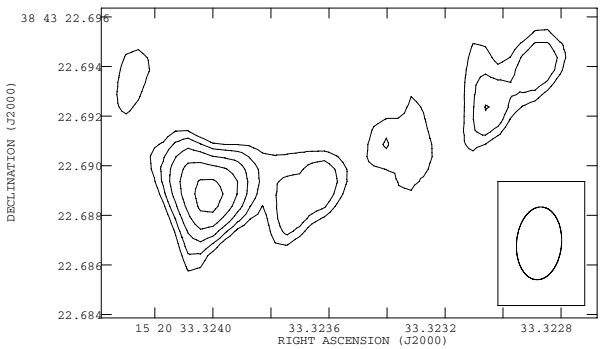

Figure 8. J1520+3843 mapped with the VLBA, using robust = 5. Contours $2.7 \times (-1, 1, \sqrt{2}, 2, 2\sqrt{2}, 4, ...)$ mJy beam^{-1}. Peak flux density 12.5 mJy beam^{-1}.

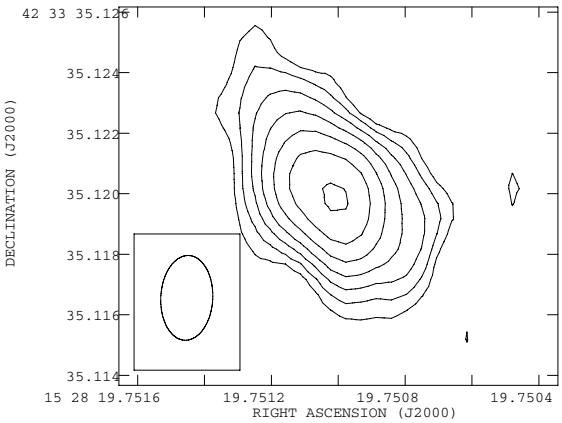

Figure 9. J1528+4233 mapped with the VLBA. Contours $2.3 \times (-1, 1, \sqrt{2}, 2, 2\sqrt{2}, 4, ...)$ mJy beam^{-1}. Peak flux density 19.2 mJy beam^{-1}.

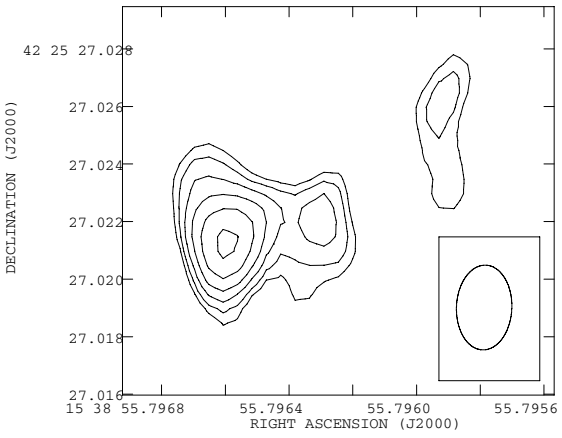

Figure 10. J1538+4225 mapped with the VLBA, using robust = 5. Contours $3.0 \times (-1, 1, \sqrt{2}, 2, 2\sqrt{2}, 4, ...)$ mJy beam^{-1}. Peak flux density 18.3 mJy beam^{-1}.

Sources are classified as steep-spectrum sources if their fitted peak frequency is below 500 MHz and the fitted spectral index at 10 GHz $\alpha_{10} > 0.5$. Following Tinti et al. (2005), we label those objects with a fitted peak frequency between 0.5 and 5.0 GHz and $A > 0.2$ as gigahertz-peaked spectrum (GPS) sources. Sources with fitted peak frequency above 5.0 GHz and with $A > 0.2$ are classified as HFP sources. Flat-spectrum sources are those with no well-defined spectral peak (with $A < 0.2$) and a fitted spectral index at 10 GHz $\alpha_{10} < 0.5$. The NASA/IPAC Extragalactic Database (NED) was searched and the spectral classification for each object was checked against archive data.[1] Extrapolation of the fitted spectra to frequencies below 1.4 GHz is somewhat speculative and the only two objects (J0925+3159 and J1510+3750) from Paper 1 with fitted peak frequencies between 0.5 and 1.0 GHz were found to have steep spectra at low frequency (151–365 MHz), suggesting that to classify them as GPS would be incorrect – both are extended, steep-spectrum objects and are classed as such. It is possible that other GPS classifications are spurious but that the sources are too faint to have any low-frequency data in NED revealing the error. There are also several 9C sources classified as HFP objects that have flat or steep spectra at low frequency in NED (e.g. J1506+4239). We do not change the spectral class of these objects, but note that although the peak seen in Paper 1 is genuine, it may be only a local maximum and not representative of the full source spectrum at the time of the observations. As mentioned in Paper 1, there are four objects in the 15^{h} sample without a simultaneous 1.4-GHz measurement, and archive data are used to help classify these objects correctly.

Examples of sources from Paper 1 in each spectral class are shown in Fig. 11.

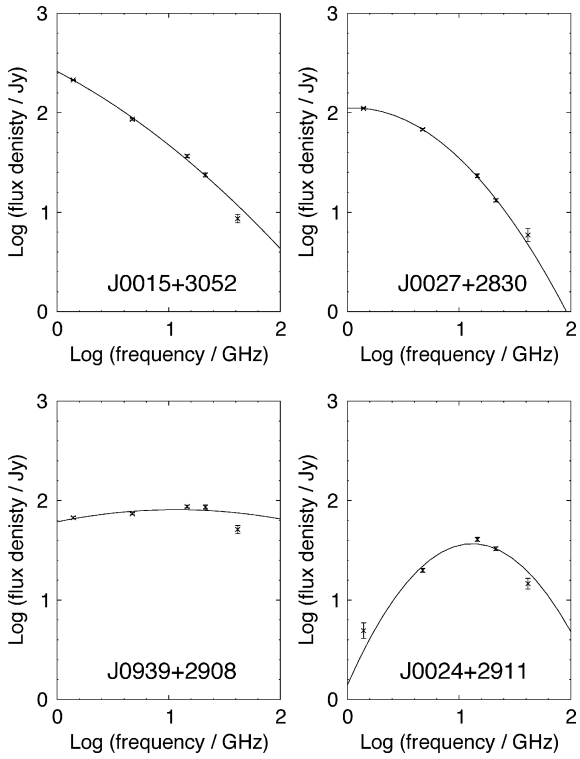

Figure 11. Examples of a steep-spectrum radio source (top left-hand panel), a GPS source (top right-hand panel), a flat-spectrum source (bottom left-hand panel) and a HFP source (bottom right-hand panel). In each plot, the black curve shows the fitted quadratic function.

4.2 Interpretation of measured flux densities

A total of six steep-spectrum objects were studied at high resolution and all have been resolved with either MERLIN or the VLBA. By contrast, only four of the 13 flat-spectrum sources, and none of the nine HFP objects or the six GPS objects, have structure resolved in the MERLIN or the VLBA data.

There is a good general correlation between the VLA-, MERLIN- and VLBA-measured flux densities but some sources have flux densities that vary significantly between observations. As mentioned previously, the sources with mapped structure have flux density measurements consistently falling at higher resolution. Table 1 also contains notes on the known or likely variability of objects. V(P3) or N(P3) in column 9 indicates that the source has been studied for variability at 15 GHz in Paper 3 and was found to vary or not to vary above ∼6 per cent at 15 GHz, respectively. Sources that show evidence for variability at 5 GHz in the NED data, and that have varying flux densities in the data presented here are labelled V(NED). A V? indicates that the flux density differs significantly between VLA/MERLIN and/or VLBA observations, but that there are no other variability data to backup the claim. One source, J1526+3712 is not found to vary in Paper 3, but shows evidence for a changing 5-GHz flux density in NED.

Sources are marked with an R in column 10 if they are resolved with mapped structure in a high-resolution map. If a source has low surface brightness extended emission from a halo (perhaps diffuse emission from relic radio lobes, or a lobe seen end-on) then this will be increasingly resolved out at higher resolution, and the measured flux density of the source will fall, even though structure may not be mapped for the source. Thus sources with flux density decreasing with increasing resolution are marked H? because their data are consistent with them having a halo.

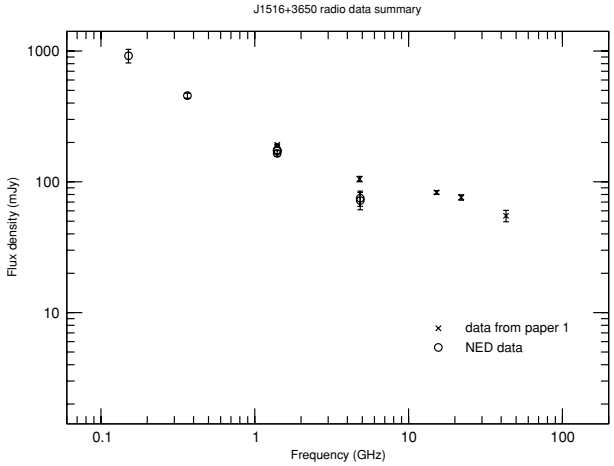

Figure 12. NED and follow-up data from Paper 1 for J1516+3650.

10 of the sources studied here are labelled H? (three HFP, two GPS and five flat-spectrum objects). Three of these (J1516+3650, J1521+4336 and J1526+3712) have steep spectra at low frequency in NED (e.g. see Fig. 12), suggesting that the emission is from a steep-spectrum component dominant at low frequency (possibly a lobe or relic lobe forming a halo) and a flat- or peaked-spectrum

[1] Spectral plots including the 9C follow-up data and variability study data are available from the FTP directory at http://www.mrao.cam.ac.uk/surveys/9C/

Table 2. The distribution of source sizes for the 61 sources in the 25-mJy flux-limited sample from the 15^h field of Paper 1. The totals are the number of objects in each size bin or spectral class. The extrapolated numbers in brackets are explained in the text.

Size bin, upper (arcsec)	<0.005	<0.05	<0.5	<2.0	<5	<20	<50		Total
Size bin, lower (arcsec)		⩾0.005	⩾0.05	⩾0.5	⩾2.0	⩾5	⩾20	⩾50	
Steep	0	3 (1)	1	4 (1)	4	7	5	3	27
GPS	7 (1)	0	0	0	0	0	0	0	7
Flat	11 (2)	4 (1)	0	1	0	1	1	0	18
HFP	9	0	0	0	0	0	0	0	9
Total	27	7	1	5	4	8	6	3	61

Table 3. The distribution of source sizes as a function of optical colour ($O - R$) for the 61 sources in the 25-mJy flux-limited sample from the 15^h field of Paper 1. The totals are the number of objects in each size bin or optical colour bin. Objects with a *lower limit* on $O - R$ of <1.6 have been included with the unidentified objects. The extrapolated numbers in brackets are explained in the text.

Size bin, upper (arcsec)	<0.005	<2.0		Total
Size bin, lower (arcsec)		⩾0.005	⩾2.0	
$O - R < 1.6$	12 (2)	5 (2)	6	23
$O - R \geqslant 1.6$	9	4 (1)	11	24
Unidentified/lower limit	6 (1)	4	4	14
Total	27	13	21	61

component dominant at higher frequency (a core or unresolved, optically thick recurrent source).

J1530+3758 is known not to vary at 15 GHz and so may well have a halo, and the remaining six H? objects are either known to vary or have no variability information. These could have haloes or be variable and decreasing in flux density over the times of the observations, or both.

4.3 Angular size distribution of the flux-limited sample

There are 61 sources in the 15^h field in the flux-limited sample A (complete to 25 mJy) of Paper 1. Of these 61, 24 have size measurements from the VLA data. 31 of the 37 sources without a VLA size measurement have been studied fully at high resolution, providing size measurements for seven previously unresolved objects, and leaving 24 unresolved even at VLBA resolution.

Table 2 shows the number of sources in different size bins found in the full 15^h, 25-mJy flux-limited sample. To take account of the six sources missed in the high-resolution follow-up extra numbers have been added to bins appropriate to their spectral type. The six which are unresolved with the VLA and not studied in full comprise two steep-spectrum sources (J1528+4219 and J1529+3945), three flat-spectrum sources (J1525+4201, J1539+4217 and J1553+4107) and one GPS source (J1556+4259).

None of the six GPS sources has been resolved so the missing one is placed in the <0.005-arcsec bin. Similarly, since nine of the 13 flat-spectrum sources observed at high resolution were smaller than 5 mas, and three are between 5 and 50 mas, we assume that two of the three unobserved ones will be <5 mas and one between 5 and 50 mas. Of the six observed steep-spectrum sources less than 2 arcsec in size but with size measurements, two are between 0.005 and 0.05 arcsec in angular extent, one is between 0.05 and 0.5 arcsec and three are between 0.5 and 2 arcsec. On the basis of this distribution, one object is added to the 0.005–0.05 arcsec bin and one to the 0.5–2 arcsec bin. The number of sources added to each bin by these extrapolations is given in brackets.

In Paper 1, we presented optical data for the sources in the 9C survey. The quality of the optical images obtained was very variable so that in our discussion of the correlation between spectral class and optical class in Paper 1, we defined optical classes on the basis of colour alone. We looked at two classes, counterparts with $O - R < 1.6$ ('blue' – possible quasars) and counterparts with $O - R \geqslant 1.6$ ('red' – galaxies), and found that the optical counterparts of the steep-spectrum sources are less often blue in colour than those of the flat- and rising-spectrum sources. Given this result and the relationship between angular size and radio spectral type apparent in Table 2, we would expect more of the sources with smaller angular sizes to be blue in colour. We have used the same optical classification scheme as in Paper 1 to look at the correlation between optical colour and angular size. The data are presented in Table 3. Only those objects, which definitely have $O - R < 1.6$, have been included in this class; objects with *lower limits* on $O - R$ of <1.6 have been included with the unidentified sources. The six sources missed in the high-resolution follow-up have been added to each bin as described above. There is one ambiguity in assigning these sources to their respective bins – a flat-spectrum source with a lower limit on $O - R$ of <1.6 – and this has been arbitrarily assigned to the <0.005-arcsec bin. The expected relationship between angular size and colour is evident in Table 3; excluding those objects which are unidentified or whose colour is undefined, 17 out of 30 (57 per cent) of the objects with angular sizes <2.0 arcsec are blue compared with six out of 17 (35 per cent) of the objects with angular sizes ⩾2.0 arcsec.

4.4 The nature of the GPS and HFP objects

Unbeamed, young sources are expected to retain peaked spectra (peaking at about 0.5 GHz or above) until they reach sizes of around 1 kpc (e.g. Snellen et al. 2000). Kiloparsec sources would all be resolved by the VLBA, regardless of their redshift, provided that the alignment angle was greater than 15° or so, which should be the case for the majority (97 per cent) of objects. Even if a source is at an angle of 10° from the line of sight (LOS), it would have to be physically smaller than 240 pc or 800 light-years (since there is a maximum of 8.5 kpc arcsec^{-1}, in the *WMAP* cosmology) to be unresolved in the VLBA data. Such a source would be younger than about 4000 yr (assuming a jet velocity of 0.2c), just 1/25 000 of its expected total lifetime of 10^8 yr.

Thus the numbers of flat-spectrum, GPS and HFP objects with very small angular sizes observed here suggest that the majority of them must be aligned very close to the LOS. This high-resolution

work rules out the possibility that all the HFP sources are young, unbeamed objects: a significant fraction, possibly all, of them are likely to be beamed. This conclusion is supported by the fact that at least six of the 16 GPS and HFP sources in this sample are associated with objects which are blue in colour and are, therefore, likely to be quasars. Up to 10 of the HFP, GPS and flat-spectrum objects could have haloes, consistent with a beaming scenario as a halo can be produced by observing a jetted source end-on. Beaming would also gives rise to variability which a significant fraction of the flat- and peaked-spectrum sources have shown in these data.

A full discussion of the implications of these data, the sample statistics from Paper 1 and the variability data will be presented in Paper 3.

ACKNOWLEDGMENTS

We are grateful to Peter Thomasson and Tom Muxlow for help observing and calibrating the MERLIN data. This work has made use of the NED, which is operated by the Jet Propulsion Laboratory California Institute of Technology, under contract with the National Aeronautics and Space Administration.

MERLIN is operated by the University of Manchester as a National Facility of the UK Particle Physics & Astronomy Research Council.

The National Radio Astronomy Observatory is a facility of the National Science Foundation operated under cooperative agreement by Associated Universities, Inc.

REFERENCES

Bolton R. C. et al., 2004, MNRAS, 354, 485 (Paper 1)
Bolton R. C., Cotter G., Pooley G. G., Riley J. M., Waldram E. M., Chandler C. J., Pearson T. J., Readhead A. C. S., submitted (Paper 3)
Fomalont E. B., Frey S., Paragi Z., Gurvits L. I., Scott W. K., Taylor A. R., Edwards P. G., Hirabayashi H., 2000, ApJS, 131, 95
O'Dea C. P., 1998, PASP, 110, 493
Snellen I. A. G., Schilizzi R. T., Miley G. K., de Bruyn A. G., Bremer M. N., Röttgering H. J. A., 2000, MNRAS, 319, 445
Taylor G. B., Vermeulen R. C., Readhead A. C. S., Pearson T. J., Henstock D. R., Wilkinson P. N., 1996, ApJS, 107, 37
Taylor A. C. et al., 2003, MNRAS, 341, 1066
Tinti S., Dallacasa D., De Zotti G., Celotti A., Stanghellini C., 2005, A&A, 432, 31
Waldram E. M., Pooley G. G., Grainge K. J. B., Jones M. E., Saunders R. D. E., Scott P. F., Taylor A. C., 2003, MNRAS, 342, 915

This paper has been typeset from a TEX/LATEX file prepared by the author.